

A porosity gradient in 67P/C-G nucleus suggested from CONSERT and SESAME-PP results: an interpretation based on new laboratory permittivity measurements of porous icy analogues

Y. Brouet,^{1★} A. C. Levasseur-Regourd,^{2★} P. Sabouroux,³ L. Neves,³ P. Encrenaz,⁴
O. Poch,¹ A. Pommerol,¹ N. Thomas,¹ W. Kofman,^{5,6} A. Le Gall,⁷ V. Ciarletti,⁷
A. Hérique,⁵ A. Lethuillier,⁷ N. Carrasco⁷ and C. Szopa⁷

¹Physics Institute, University of Bern, Sidlerstrasse 5, CH-3012 Bern, Switzerland

²UPMC (Sorbonne Univ.); UVSQ (UPSay); CNRS/INSU; LATMOS-IPSL, BC 102, 4 place Jussieu, F-75005 Paris, France

³Aix-Marseille Université, CNRS, Centrale Marseille, Institut Fresnel, UMR 7249, Campus universitaire de Saint-Jérôme, avenue Escadrille-Normandie-Niemen, F-13013 Marseille, France

⁴LERMA, Paris Observatory, F-75014 Paris, France

⁵UGA-Grenoble CNRS-INSU, Institut de Planétologie et d'Astrophysique de Grenoble UMR 5274, F-38058 Grenoble, France

⁶Space Research Center, PAS, F-00-716 Warsaw, Poland

⁷UVSQ (UPSay); UPMC (Sorbonne Univ.); CNRS/INSU; LATMOS-IPSL, 11 boulevard d'Alembert, F-78280 Guyancourt, France

Accepted 2016 August 23. Received 2016 August 22; in original form 2016 June 19

ABSTRACT

The *Rosetta* spacecraft made a rendezvous with comet 67P/Churyumov-Gerasimenko (67P) in 2014 August, soon after the Philae module landed on the small lobe of the nucleus on 2014 November 12. The CONSERT instrument, onboard *Rosetta* and Philae, sounded the upper part of the interior of 67P with radiowaves at 90 MHz and determined an average of the real part of the permittivity (hereafter ϵ') equal to about 1.27. The SESAME-PP instrument, onboard Philae, sounded the near-surface of the small lobe in the 400–800 Hz range and determined a lower limit of ϵ' equal to 2.45. We use a semi-empirical formula obtained from measurements of ϵ' performed in the laboratory at 243 K on water ice and ice-basaltic dust mixtures, with a controlled porosity in the 31–91 per cent range and a dust-to-ice volumetric ratio in the 0.1–2.8 range, to interpret the results of the two instruments, taking into account the temperature and frequency dependences. A graphical method is proposed to derive ranges of porosity and dust-mass fraction from a value of ϵ' derived from observations. The non-dispersive behaviour of ϵ' below 175 K, allows us to compare the values of ϵ' obtained by CONSERT and SESAME-PP. We show that the porosity of the small lobe of 67P increases with depth. Based on new measurements of analogues of complex extraterrestrial organic matter, the so-called *tholins*, we also suggest that, for the dust component in the cometary material, the presence of silicates has more effect on ϵ' than organic materials.

Key words: methods: data analysis – methods: laboratory: solid state – space vehicles: instruments – comets: general – comets: individual: 67P/Churyumov-Gerasimenko.

1 INTRODUCTION

The European Space Agency's *Rosetta* spacecraft made a rendezvous with comet 67P/Churyumov-Gerasimenko (hereafter 67P) at the beginning of 2014 August. The Philae lander was released from *Rosetta* on 2014 November 12 and landed finally, after three rebounds, on the Northern hemisphere of the small lobe of the nu-

cleus (Biele et al. 2015). High-resolution observations of the nucleus have been acquired with the Optical, Spectroscopic, and Infrared Remote Imaging System (OSIRIS; Keller et al. 2007) revealing the morphological diversity of the comet's surface (Thomas et al. 2015). Many features of the surface of the nucleus have been already described in the 19 regions defined in the Northern hemisphere (see e.g. Auger et al. 2015; El-Maarry et al. 2015a,b; Groussin et al. 2015; Sierks et al. 2015; Thomas et al. 2015); for instance smooth deposits, consolidated materials, isolated boulders, depressions, cliffs, layering, and fractures. The generally dehydrated nature of the surface has been suggested by measurements performed

★ E-mail: yann.brouet@space.unibe.ch (YB);
Anny-Chantal.Levasseur-Regourd@latmos.ipsl.fr (ACL-R)

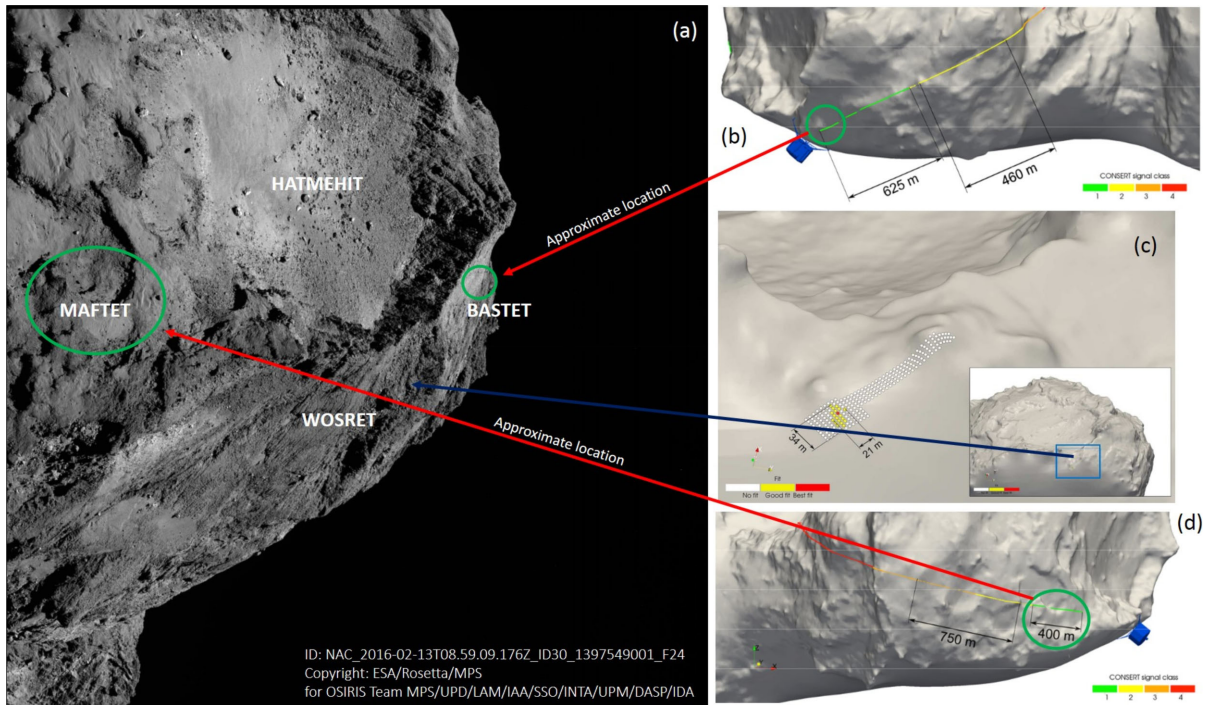


Figure 1. a: OSIRIS narrow-angle camera image taken on 2016 February 13. The scale is $0.82 \text{ m pixel}^{-1}$. It shows the Hatmehit region and partially the Maftet, the Wosret and the Bastet regions. The green circles show approximately the locations where the CONSERT signals of class one have crossed the surface of the 67P nucleus during the FSS. b and d: east and west parts of the small lobe on the shape model of the nucleus. The coloured lines show the different CONSERT signals (figures modified from Kofman et al. 2015). c: hypothetical landing sites of the Philae lander marked by dots on the shape model (figure modified from Kofman et al. 2015).

by the Visible, InfraRed, and Thermal Imaging Spectrometer (VIRTIS; Coradini et al. 2007) between 2014 August and September (Capaccioni et al. 2015), although about one hundred metre-sized bright spots have been identified during the pre-perihelion observations with the OSIRIS instrument and have been interpreted as exposures of water ice (Pommerol et al. 2015), an interpretation later confirmed by VIRTIS for some of the largest outcrops (Filacchione et al. 2016). As expected from previous studies, the cometary nucleus is composed of ices (mostly water) and refractory materials (hereafter dust). The dust-to-gas mass ratio, averaged over the sunlit nucleus surface by the Grain Impact Analyser and Dust Accumulator (GIADA; Rotundi et al. 2015) before perihelion, was found to be about (4 ± 2) . The dust component is expected to be mostly composed of crystalline and glassy silicate minerals, organic molecules, iron sulfides and FeNi alloys (e.g. Festou, Keller & Weaver 2004; Cochran et al. 2015). The observations of the surface of 67P by VIRTIS mostly indicate the presence of refractory organic compounds mixed with opaque minerals, which may consist of FeNi alloys and iron sulfides (Capaccioni et al. 2015; Quirico et al. 2016).

While the physical and chemical properties of the surface have been studied by several instruments, properties of the interior can only be assessed by the Radio Science Investigation (RSI; Pätzold et al. 2007) and the Comet Nucleus Sounding Experiment by Radiowave Transmission (CONSERT; Kofman et al. 1998). From measurements of spacecraft velocity perturbations, Pätzold et al. (2016) have derived the gravity field and mass of the nucleus to constrain the internal structure of the nucleus with RSI. Knowing the current estimate of the volume of the nucleus, they have estimated an average value for the bulk density of the nucleus equal to about 533 kg.m^{-3} . They have also suggested that large voids within the nucleus (macroporosity) can be excluded. The

interior of the nucleus is homogeneous at global scales. CONSERT is a bistatic penetrating radar operating at a centre-band frequency equal to 90 MHz. It uses the transmission of an electromagnetic wave through the cometary nucleus, between the Philae lander and the *Rosetta* orbiter, to derive internal properties. CONSERT acquired data during the evening of 12 November and the morning of 13 of November 2014 during the First Science Sequence (hereafter FSS). Kofman et al. (2015) used the CONSERT signals of ‘class one’, i.e. displaying a strong signal-to-noise ratio and a good synchronization, to constrain the internal properties of the nucleus over a depth of hundred of metres. The CONSERT signals of ‘class one’ have partially crossed the regions of the small lobe of the nucleus named Bastet and Maftet defined in the Northern hemisphere by El-Maarry et al. (2015b), as shown in Fig. 1. The Maftet and Bastet regions have been identified as strongly consolidated regions (El-Maarry et al. 2015b). Moreover, CONSERT has been able to contribute to refine the location of the Philae lander (Hérique et al. 2015; Kofman et al. 2015). The suggested final landing site of Philae, named Abydos, is likely to be within a strip measuring approximately 34 by 21 m². This strip is located between the Wosret region, defined in the Southern hemisphere of the nucleus once it was illuminated by sunlight, and the Hatmehit region characterized by a depression (El-Maarry et al. 2015b) in the Northern hemisphere. The Southern hemisphere seems to lack smooth terrains and dust coatings, and would closely resemble the Northern hemisphere consolidated regions (El-Maarry et al. 2016).

The near-surface (first metre) of the small lobe has been sounded by the permittivity probe (hereafter PP), which is part of the Surface Electric Sounding and Acoustic Monitoring Experiment (SESAME; Seidensticker et al. 2007) package, at the final landing site of Philae. SESAME-PP consists of three transmitting electrodes and two

receiving electrodes operating between 10 Hz and 10 kHz. Three of them are located on the feet of the Philae lander and the two other are co-located with parts of the MULTI PUrpose Sensors for surface and subsurface Science (MUPUS; Spohn et al. 2007) and Alpha Particle X-Ray Spectrometer (APXS; Klingelhofer et al. 2015) instruments. As well as CONSERT, SESAME-PP operated during the FSS (Lethuillier et al. 2016).

CONSERT and SESAME-PP use radiowaves within different frequency bands to sound the cometary material. The interaction of electromagnetic waves with a non-magnetic medium, as suggested for 67P (Auster et al. 2015), is described by the relative complex permittivity ϵ (hereafter permittivity) of the medium, relative to that of vacuum ϵ_0 ($=8.854 \times 10^{-12} \text{ F m}^{-1}$), which is defined as: $\epsilon = \epsilon' - j\epsilon''$. The real part, ϵ' , represents how much of energy from an electromagnetic wave is stored in the medium. The imaginary part, ϵ'' , is proportional to the electrical conductivity of the medium and represents the loss by absorption in the medium. ϵ' and ϵ'' describe the polarization mechanisms acting in a medium crossed by an electrical field. All polarization mechanisms, including electronic, atomic, orientation and space charge polarizations (e.g. Ulaby & Long 2014), occur at low frequencies, where it is easier for dipoles and charge carriers to follow the variations of the electric field, hence a greater ϵ' at low frequencies. Only electronic and atomic polarizations can act and contribute to the value of ϵ' when the frequency increases because of their small relaxation time. The electrical energy is dissipated into heat in the medium by the polarization mechanisms, leading to an increase of ϵ'' at high frequencies. Thus, the permittivity of a medium is dependent on its composition and on the frequency of measurement. For instance, the permittivity of solid water ice shows a real part equal to about 100 at 250 K at low frequencies, i.e. lower than 1 MHz, whereas its high-frequency limit is about 3.1–3.2 (e.g. Mätzler & Wegmüller 1987; Mattei et al. 2014). Campbell & Ulrichs (1969) performed measurements on basaltic rocks at 450 MHz and 35 GHz and have determined a real part of the permittivity in the range of 5–10 and an imaginary part in the range of 0.02–0.90. However when the temperature of the medium decreases, the polarization mechanisms become less efficient, even at low frequencies. Indeed, the dipoles and charge carriers react more slowly to the variations of the electrical field and their relaxation time become larger. Also, Mattei et al. (2014) have experimentally highlighted the non-dispersive behaviour of ϵ' for pure solid water ice and water ice/basaltic dust mixtures between 20 and 1 MHz at temperature below 175 K. In this particular condition of temperature, ϵ' remains equal to its high-frequency limit at low frequencies. For powdered and porous media, such as volcanic ashes, porous ices, or rocks reduced in powder, the permittivity is also dependent on bulk density (i.e. the mass of material normalized by the occupied volume) and the porosity (i.e. the volume fraction of empty space in a given volume): ϵ' and ϵ'' increase with the increasing bulk density (Campbell & Ulrichs 1969; Olhoeft & Strangway 1975; Heggy et al. 2001; Brouet et al. 2014) and decrease with the increasing porosity (Heggy et al. 2001; Brouet et al. 2015). Thus, the permittivity depends on the frequency of the applied electrical field, the composition, the temperature and the porosity of the medium.

From propagation time analyses of the radiowaves at 90 MHz between the Philae lander and the *Rosetta* orbiter, Kofman et al. (2015) have estimated the mean value of the real part of the permittivity of the small lobe of the nucleus at 90 MHz: 1.27 ± 0.05 . They have interpreted this result with a method based on the computation of the effective permittivity of various ice and dust mixtures with different porosities using the Hashin–Shtrikman bounds

(Sihvola 1999) derived from Maxwell Garnett mixing formulae, with assumptions regarding the dust and ice composition for which the permittivity values have been measured (see e.g. Pettinelli et al. 2003; Andersson 2008; Heggy et al. 2012). Thanks to this method, Kofman et al. (2015) suggest that the porosity of the upper part of the small lobe is in the range of 75–85 per cent and the ice-to-dust volumetric ratio in the range of 0.1–2.6. From the analysis of SESAME-PP data, Lethuillier et al. (2016) have provided a lower limit of the real part of the permittivity of 2.45 ± 0.20 in the frequency range of 409–758 Hz for the first metre of the near-surface at Philae’s location. Using the same approach as Kofman et al. (2015) and assuming that the dust component consists of carbonaceous chondrites, Lethuillier et al. (2016) estimate a porosity of at most 55 per cent for the near-surface and thus conclude on an increase of the porosity with depth.

We report in this paper on a different method of interpretation of the results obtained by Kofman et al. (2015) and Lethuillier et al. (2016), relying on new laboratory measurements of porous and icy cometary analogues and on a semi-empirical formula obtained from these measurements. Brouet et al. (2016) have constrained the real part of the permittivity of porous water ice samples and porous water ice-dust mixtures as a function of the dust content and the porosity of the samples for frequencies in the range of 50 MHz–2 GHz at a temperature equal around 243 K. The dust components are samples of JSC-1A Lunar regolith simulant with a mean grain size lower than 125 μm , which mostly consists of non-hydrated silicate minerals such as plagioclase, pyroxene and olivine. From the extensive spectral mapping of VIRTIS of the surface, no hydrated minerals were identified (Capaccioni et al. 2015; Quirico et al. 2016). Therefore their intrinsic porosity and their chemical properties make them suitable to be considered as an analogue for porous cometary dust of 67P. First, we define how these laboratory measurements can be applied to the investigation of the internal and near-surface properties of the small lobe of the nucleus, taking into account the temperature conditions during the measurements of SESAME-PP and CONSERT. Then we study the effects of the composition of the dust component on ϵ' by comparing the measurements performed with the silicate-rich materials and new measurements performed on organic compounds. Secondly, using this approach, we highlight an increase of the porosity with the increasing depth in the small lobe of the 67P nucleus, which supports the conclusions presented in Lethuillier et al. (2016).

2 LABORATORY MEASUREMENTS RELEVANT TO CONSERT AND SESAME-PP DATA

2.1 Temperature range

During the FSS, the temperature sensors of the SESAME package have determined the temperature of the surface at the landing site of Philae to be in the range of 100–150 K (Lethuillier et al. 2016). These measurements are consistent with those of the MUPUS-TM (Thermal Mapper) instrument, which measured a diurnal temperature between 90 and 130 K at the landing site (Spohn et al. 2015). Regarding the temperature of the interior of the nucleus, clues can only be inferred from computational modelling. In the interior of the cometary nucleus, temperatures are expected to be of the order of 100 K and possibly lower (e.g. Festou et al. 2004). These predicted values of temperatures at depth are also supported by *in situ* determination of the thermal inertia. Indeed, Spohn et al. (2015) have found that the best model to fit the temperature monitored by MUPUS-TM is reached for a thermal inertia equal to

$85 \pm 35 \text{ J m}^{-2} \text{ K}^{-1} \text{ s}^{-1/2}$. Moreover, a very low thermal inertia has been determined by the MIRO radiometer at shallow depths in the range of $10\text{--}50 \text{ J m}^{-2} \text{ K}^{-1} \text{ s}^{-1/2}$ for the overall subsurface of the nucleus (Gulkis et al. 2015). These results mean that the near-surface of the nucleus is a very good insulator. Consequently, the deep material in the nucleus would be very weakly sensitive to the thermal waves induced by the variation of solar illumination.

Thus, we can reasonably assume that the temperatures in the interior of the small lobe and in the near-surface at Abydos were below 150 K during FSS measurements and that the temperature difference was less than 100 K.

2.2 Laboratory measurements on porous icy analogues

In order to link the electrical properties of the small lobe of the nucleus measured by CONSERT and SESAME-PP to physical properties, we have chosen to focus on an approach strictly based on experimental data. These data have been obtained from permittivity measurements of analogue materials consisting of porous silicate-rich dust mixed with a porous Ih crystalline water ice. In 2014 November, we performed laboratory measurements of the permittivity of porous silicate-rich dust in the range of 50–6 GHz, encompassing the operating frequency of CONSERT, under ambient temperature (around 300 K) and pressure conditions (Brouet et al. 2015). Then in 2015 October and December, we performed permittivity measurements on porous water ice and water ice-dust mixtures in the frequency range of 50–2 GHz, at a temperature around 243 K and under ambient pressure (Brouet et al. 2016). The same experimental setup, which consists of a coaxial cell connected to a vector network analyzer, has been used for these three campaigns of measurements. For each frequency, the permittivity is determined as the mean of the permittivity obtained from the S-parameters S_{11} and S_{21} (i.e. the reflection coefficient measured at one port of the coaxial cell and the transmission coefficient measured at the other port) and the permittivity obtained from the S-parameters S_{22} and S_{12} . The Nicolson–Ross algorithm is used to relate the S-parameters to the permittivity (Nicolson & Ross 1970). The good matching between the results obtained from S_{11} and S_{21} and the results obtained from S_{22} and S_{12} testify of the homogeneity of the samples. This setup has allowed us to follow strictly the same procedure of measurement and the same procedure of sample preparation for each measurement, thus ensuring a good reproducibility of the permittivity measurements.

The dust component studied during these campaigns of measurements is the JSC-1A Lunar regolith simulant (Hill et al. 2007). It mostly consists of tiny crystallized grains, as well as dark and basaltic porous grains composed of non-hydrated silicate minerals. It is suitable to be considered as an analogue of porous cometary dust of 67P. It had been split into six subsamples with different size distributions between a few microns and 600 μm . The bulk density of these samples ranges between 1000 and 1500 kg.m^{-3} . The porosity of these samples has also been derived from the bulk density values and estimated to be between 50 and 63 per cent, given the solid density of the JSC-1A simulant equal to 2.92.

For the last two measurement campaigns, quasi-spherical ice particles have been produced by two different techniques using the SPIPA (Setups for Preparation of Icy Planetary Analogues) setups at the Physics Institute of the University of Bern. A first technique is based on the vaporization of deionized water to form very fine droplets. These droplets are conducted through a plastic tube inside a chest freezer at a temperature equal to about 223 K. Then the droplets condense to form fine-grained ice particles with a mean size

equal to $4.5 \pm 2.5 \mu\text{m}$ (Jost et al. 2016). A second technique is based on the atomizing of liquid deionized water into microdroplets using an ultrasonic unit equipped with a sonotrode, which takes place inside a chest freezer at the same temperature as the first technique. Then the droplets condense to form coarse-grained ice particles with a mean size equal to about $67 \pm 31 \mu\text{m}$ (Yoldi et al. 2015; Poch et al. 2016b). The porosities of samples composed of fine-grained ice and coarse-grained ice have been, respectively, determined to be between 49 and 86 per cent and between 31 and 50 per cent.

In order to prepare the water ice-dust mixtures, a subsample of the JSC-1A simulant, with a mean grain size equal to $24 \pm 9 \mu\text{m}$, has been mixed with the fine-grained ice according to a controlled and reproducible procedure. Another subsample of the JSC-1A simulant, with a mean grain size equal to be about $74 \pm 28 \mu\text{m}$, has been mixed with the coarse-grained ice. The porosity of the ice-dust mixtures during the permittivity measurements have been derived to be between 42 and 91 per cent. The dust-mass fraction, i.e. the ratio of the dust mass to the total mass of the sample, has been estimated to be between 0.25 and 0.90, meaning a dust-to-ice volumetric ratio in the range of 0.1–2.8, given the solid density of the two components.

The properties of these porous icy analogues are presented in supplementary materials of this paper.

2.3 Modelling ϵ' as a function of porosity, dust content and temperature from experimental data

Amongst other results to be presented in Section 2.5, Fig. 2 shows the averaged values of ϵ' obtained in the frequency range of 50 MHz–2 GHz as a function of porosity for pure dust component (i.e. the JSC-1A simulant) as well as pure water ice samples and ice-dust mixtures mentioned above with dust-to-ice volumetric ratios in the range of 0.1–2.8.

For the water ice samples and ice-dust mixtures, ϵ' decreases with increasing porosity Φ and the trend can be modelled as follows: $A^{(1-\Phi)}$, with A the fitting parameter. This model is derived from the Lichtenecker formula, which expresses the logarithm of the effective permittivity of a mixture as the sum of the products of the volume fraction and the logarithm of the permittivity of each component (see e.g. Olhoeft & Strangway 1975). The A parameter increases with the increasing dust-mass fraction, so that its value as a function of the dust-mass fraction can be modelled by a second-order polynomial law. Thus, a semi-empirical formula has been derived from these measurements. From this formula, ϵ' can be estimated as a function of any porosity Φ and any dust-mass fraction F_D for materials composed of water ice and/or silicate-rich materials, as the JSC-1A Lunar simulant. It is valid for a temperature around 243 K and for a frequency range between 50 MHz and 2 GHz. The formula is written as follows:

$$\epsilon'(F_D, \Phi, T) = (5.65 \times F_D^2 - 0.23 \times F_D + 3.22)^{1-\Phi}. \quad (1)$$

In the context of the investigation of internal properties of the small lobe of 67P, the slight dependence of the permittivity with the temperature has to be taken into account. Indeed, equation (1) is valid around 243 K, whereas the temperatures at the near-surface of Abydos site and the interior of the small lobe during the FSS were lower than 150 K as mentioned in Section 2.1. Mattei et al. (2014) have shown that from 250 to 150 K, the temperature dependence of the permittivity of water ice/basaltic dust mixtures with porosities of 5 and 11 per cent decreases with the increasing frequency. At 1 MHz, the real part of the permittivity varies by about $2 \times 10^{-3} \text{ K}^{-1}$. Mätzler & Wegmüller (1987) have also shown that the real part of the permittivity of solid water ice is independent of

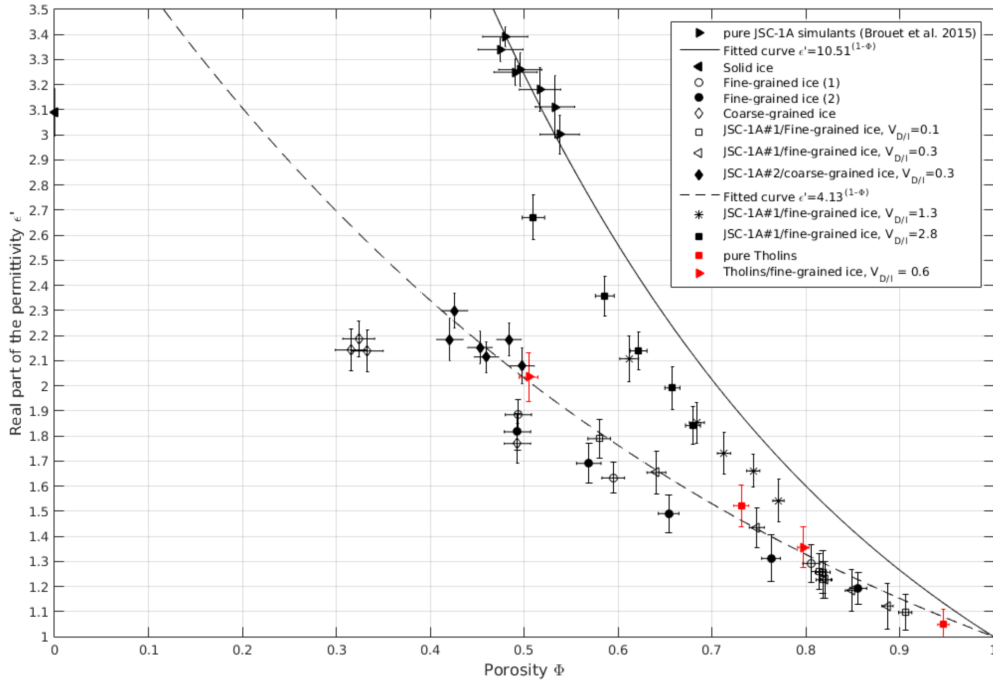


Figure 2. Real part of the permittivity, averaged over frequencies between 50 MHz and 2 GHz, decreasing with the increasing porosity Φ . This figure is modified from Brouet et al. (2016) which shows data obtained on pure fine-grained and coarse-grained ice samples and ice-dust mixtures. The additional data presented correspond to two samples composed of pure tholins (red squares) and two mixtures composed of tholins and fine-grained ice with a dust-to-ice volumetric ratio equal to 0.6 (red triangles).

frequency from 10 MHz to 300 GHz and only slightly and linearly dependent on temperature with a slope equal to $9.1 \times 10^{-4} \text{ K}^{-1}$ providing a maximum value of 3.19 at 273 K, in agreement with results from Gough (1972). Moreover, Calla & Rathore (2012) have shown that the real part of the permittivity of the JSC-1A simulant increases linearly with the increasing temperature and varies by $(2.6 \pm 0.2) \times 10^{-3} \text{ K}^{-1}$ at 1.7 GHz. Thus, the slope of the linear temperature dependence of the real part of the permittivity determined in equation (2) has been estimated to be of the order of 10^{-3} in the frequency range of our measurements.

Then, to define the real part of the permittivity as a function of the porosity, the dust-mass fraction and the temperature for materials composed of water ice and/or silicate-rich materials and for a frequency range between 50 MHz and 2 GHz, equation (1) can be modified as follows:

$$\epsilon'(F_D, \Phi, T) = (5.65 \times F_D^2 - 0.23 \times F_D + 3.22)^{1-\Phi} + (T - 243) \times 10^{-3}. \quad (2)$$

Equation (2) allows us to assess ϵ' for the estimated temperatures of the nucleus during the FSS. At a temperature equal to 100 K, the estimated ϵ' can be representative of the values of ϵ' at 150 and 50 K with plus or minus 3 per cent of variation. This encompasses the expected range of temperature in the interior of the small lobe as well as the temperature measured at Abydos during the FSS. Fig. 3 shows the isolines of ϵ' as a function of the porosity and the dust-mass fraction obtained from equation (2) at a temperature equal to 100 K. From a given value of ϵ' in Fig. 3, one can estimate the different combinations of values of porosity and dust-mass fraction. For instance, for a temperature equal to 100 K, a real part of the permittivity equal to 1.5 means that the porosity can vary from 57 to 77 per cent for any value of dust-mass fraction.

2.4 Constraints on ϵ'' for porous icy analogues

The measurements of the imaginary part of the permittivity of the porous icy analogues suggest that it is very small, because it is lower than the sensitivity limit of the instrument which is equal to about 0.1.

At a temperature of about 300 K, the imaginary part of the permittivity of volcanic ashes of basaltic composition have been performed by Calla & Rathore (2012) at 1.7 GHz and Adams et al. (1996) in the frequency range of 4–19 GHz, respectively. With similar temperature conditions, Heggy et al. (2001) and Campbell & Ulrichs (1969) have performed measurements on powdered basalts at 2 and 450 MHz, respectively. The non-dispersive behaviour of ϵ'' for frequencies greater than 10 kHz suggested from measurements on dry volcanic ashes performed by Mattei et al. (2014) allows us to compare these measurements obtained at different frequencies. Fig. 4 suggests that, at about 300 K and for a porosity larger than 65 per cent, ϵ'' may be lower or equal to about 0.01 at the operating frequency of CONSERT. For a mixture composed of water ice and silicate-rich materials, taking into account the decrease of ϵ'' with the increasing porosity and decreasing temperature (Heggy et al. 2001; Calla & Rathore 2012; Ulaby & Long 2014), and because of the relative transparency of the water ice to the radiowaves (Mätzler & Wegmüller 1987; Mattei et al. 2014), it is reasonable to assume that ϵ'' would probably be close to 0.001 at temperatures around 100 K.

2.5 Laboratory measurements on tholins, as analogues of extraterrestrial organic compounds

The empirical model, from which Fig. 3 is obtained, takes into account a dust component which mostly consists of non-hydrated silicates. But comets are also known to contain a large quantity of organic matter (e.g. Festou et al. 2004; Cochran et al. 2015, and

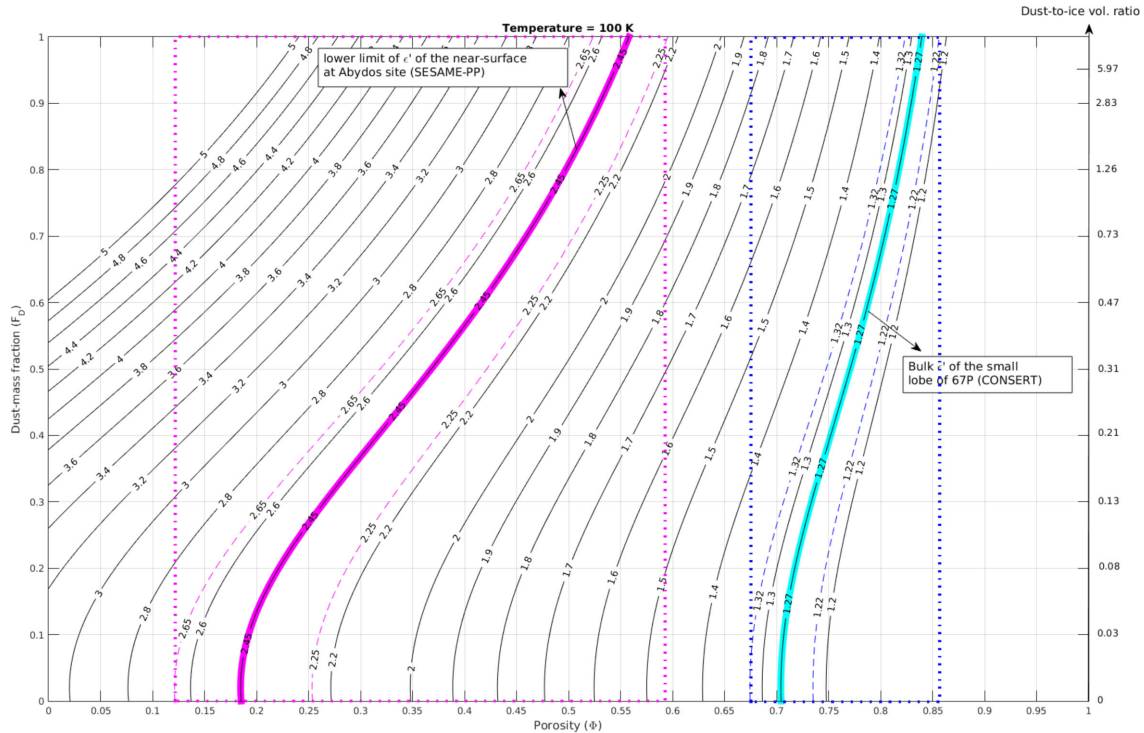


Figure 3. Isolines of the real part of the permittivity for a temperature equal to 100 K as a function of the dust-mass fraction and porosity, determined from equation (2), for mixtures composed of water ice and silicate-rich materials as the JSC-1A Lunar simulant. The red isoline represents the lower limit of ϵ' determined by SESAME-PP in the near-surface of the small lobe of 67P at Philae landing final site during the FSS and the dotted red isolines are the lower and upper limits of this value. The blue isoline represents the bulk value of ϵ' of the small lobe, taking into account the values of ϵ' in the interior (i.e. about hundred of metres) as determined by CONCERT, and the dotted blue isolines are the lower and upper limits of this value. The absence of intersection of the likely porosities between the subsurface and the interior of the small lobe indicates an increase of the porosity as a function of the depth, possibly either continuous or discontinuous.

references therein). In order to constrain the effect of the composition of the expected cometary dust component on the real part of the permittivity, we performed new measurements in 2015 December between 50 MHz and 2 GHz, and at a temperature around 243 K, with so-called tholins as tentative analogues of the solid organic matter present on cometary nuclei.

2.5.1 Sample preparation

To perform the measurements, a large amount (of the order of the gram) of tholins was required. The existing setups producing tholins from the irradiation of ices produce thin films consisting of only some micrograms of organic residue. In contrast, the irradiation of gases can produce one gram of tholins within 30–100 h depending on the gas mixture (Sciamma-O’Brien et al. 2010). For this reason, we chose to use tholins produced in the gas phase with the PAMPRE setup (Production d’Aérosols en Microgravité par Plasmas REactifs; Szopa et al. 2006) at LATMOS laboratory (France). Moreover, the physico-chemical properties of the tholins produced by PAMPRE have been characterized by several previous studies (e.g. Carrasco et al. 2009; Mahjoub et al. 2012; Sciamma-O’Brien et al. 2012).

The production of tholins with this setup is based on the irradiation of a gaseous mixture in a radiofrequency capacitively coupled plasma (Szopa et al. 2006). The tholins used in this study were produced at an incident power of 30 W and from a gaseous mixture of 95 per cent nitrogen N_2 and 5 per cent methane CH_4 . These tholins

consist of a complex mixture of molecular and macromolecular material, partly heteropolymer-like, containing carbon, hydrogen and nitrogen atoms and have a spherical shape with a mean diameter equal to 315 ± 185 nm (Carrasco et al. 2009; Pernot et al. 2010). They are considered as analogues of organic matter produced by photodissociation in the atmosphere of Saturn’s moon Titan.

In the context of comets, Bonnet et al. (2015) have shown that these tholins may be interesting precursors to simulate the nitrogen-rich inclusions in stratospheric interplanetary dust particles (IDPs) and carbonaceous Antarctic micrometeorites, which may originate from cometary nuclei (Duprat et al. 2010; Nesvorný et al. 2010). Many nitrogen-bearing organic compounds have been detected by the Cometary Sampling and Composition (COSAC; Goesmann et al. 2007) experiment on *Rosetta*’s lander Philae, such as amines, nitriles, amides and isocyanates (Goesmann et al. 2015).

However, reflectance spectra of the surface of 67P obtained by VIRTIS are inconsistent with the presence of large amount of amines and the bulk of the organic matter in most IDPs has a low abundance of nitrogen (see Quirico et al. 2016, and references therein). So the nitrogen-rich tholins used in this study are one possible analogue, but nitrogen-poor tholins, whose production in large quantity is more challenging, will also have to be considered for future measurements.

The bulk density of these samples has been measured during the permittivity measurements by weighing the filled sample holder, knowing the mass of the empty sample holder and its useful volume, equal to 1.291 ± 0.288 cm³. Also, for the first time, the solid

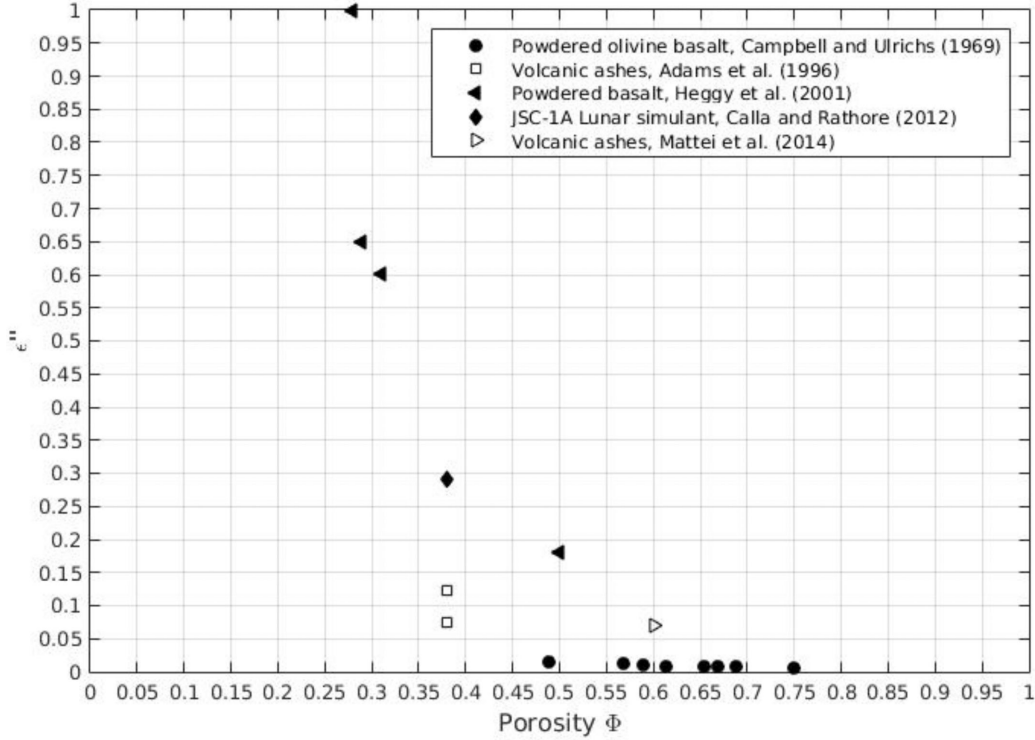


Figure 4. Decrease of the imaginary part of the permittivity of powdered basalts and volcanic ashes of basaltic composition with the increasing porosity. All the measurements have been performed at frequencies greater than 1 MHz, for which the frequency dependence of ϵ'' is expected to be negligible (Mattei et al. 2014).

density of these tholins has been measured with a helium pycnometer Upyc-1200e-V5.04 in order to determine the porosity of the samples. The solid density of the tholins is equal to 1.44 ± 0.01 . This value is similar to the one measured by Imanaka et al. (2012) which is equal to about 1.3. The porosity of pure samples can be determined by $(1 - \rho/(1000 \times \rho_s))$, where ρ is the bulk density (kg.m^{-3}) and ρ_s is the solid density of the material. The values of porosity vary between 73 and 95 per cent for compacted and non-compacted samples composed of pure tholins, respectively. For ice-dust mixtures the porosity Φ can be determined by

$$\Phi = 1 - \frac{\rho}{1000} \times \left(\frac{F_D}{\rho_D} + \frac{1 - F_D}{\rho_I} \right), \quad (3)$$

with F_D the dust-mass fraction, ρ_I the solid density of the fine-grained ice (equal to 0.917 for Ih-type crystalline water ice; e.g. Lide 2005) and ρ_D the solid density of the dust component, which refers to any refractory material.

The properties of the samples are summarized in the Table 1.

2.5.2 Results

Fig. 5 shows the real part of the permittivity for the samples composed of pure tholins and mixtures composed of fine-grained water ice and tholins, with a dust-to-ice volumetric ratio equal to 0.6, as a function of the measurement frequency on a logarithmic scale between 50 MHz and 2 GHz. The values of ϵ' vary by less than 10 percent over the frequency range of measurement. The non-dispersive behaviour of ϵ' for these samples is similar to the one measured for pure solid water ice and silicate-rich materials (Mätzler & Wegmüller 1987; Mattei et al. 2014; Brouet et al. 2015) at frequencies greater than 1 MHz.

For a non-compacted sample, ϵ' is determined to be below 1.1, showing that the sample is highly porous. This result is also in agreement with the results obtained by Paillou et al. (2008) who have conducted permittivity measurements, at 13 GHz and at a temperature of 77 K, on pure tholins samples produced with PAMPRE from a 2 per cent methane atmosphere. They obtained the following results regarding the complex permittivity: $\epsilon = 1.17 - j0.0033$ for a non-compacted sample and $\epsilon = 2.33 - j0.0206$ for a compacted sample. These measurements highlight the high porosity of such non-compacted tholin samples.

Fig. 2 shows the averaged values of ϵ' obtained in the frequency range of 50 MHz–2 GHz as a function of the porosity for the samples composed of pure tholins and the mixtures composed of fine-grained water ice and tholins if the trend of increase with the decreasing porosity from the pure tholins measurements is taken into account. Fig. 2 allow us to compare the effect of the composition on ϵ' between silicate-rich materials and complex organic materials. For this purpose, samples with similar porosities have to be compared. The values of ϵ' for the samples composed of pure tholins are smaller than those predicted for the pure JSC-1A simulant from the regression analysis for the same porosity. For instance for a porosity equal to about 73 per cent, ϵ' is greater by about 24 per cent for the pure JSC-1A simulant, with a negligible effect of the temperature. Moreover, according to the data presented in Fig. 2, ϵ' of the solid material, obtained for a null porosity, is estimated to be 10.5 for the JSC-1A Lunar simulants and at least twice less for the tholins, if the trend of the increase of epsilon with the decreasing porosity from the pure tholins measurements is taken into account. These first results suggest that the effect of silicate-rich materials on ϵ' is dominant with respect to organic materials.

Table 1. Sample properties: ϕ , the grain size distribution; F_D , the dust-mass fraction; $[D/I]_V$, the dust-to-ice volumetric ratio; m , the mass of sample inside the sample holder; ρ , the bulk density and $\delta\rho$ its uncertainty; Φ , the porosity and $\delta\Phi$ its uncertainty. The uncertainties on the bulk density and the porosity values have been assessed by using the method of error propagation.

Sample	ϕ (μm)	F_D	$[D/I]_V$	$m \pm 10$ (mg)	$\rho \pm \delta\rho$ (kg.m^{-3})	$\Phi \pm \delta\Phi$ (per cent)
Tholins	0.1–0.5			100	77 ± 8	94.6 ± 0.6
Tholins	0.1–0.5			500	387 ± 12	73.1 ± 0.8
Tholins/fine-grained ice	0.1–0.5/2–7	0.48	0.6	290	225 ± 9	79.8 ± 0.6
Tholins/fine-grained ice	0.1–0.5/2–7	0.48	0.6	710	550 ± 15	50.4 ± 1.0

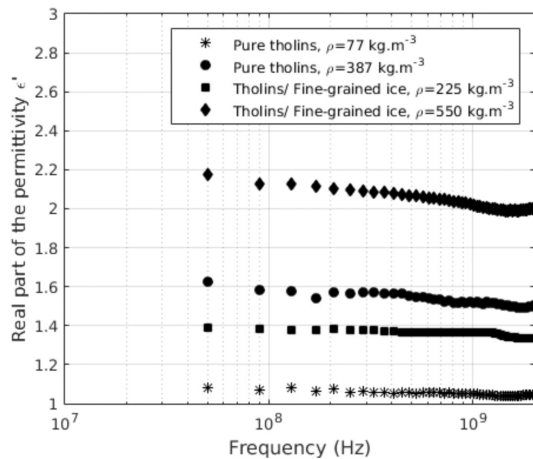


Figure 5. Real part of the permittivity as a function of the frequency for two samples composed of pure tholins and two mixtures composed of tholins and fine-grained ice with a dust-to-ice volumetric ratio equal to 0.6. The errors on the measurements were estimated to be equal or less than 10 per cent.

3 IMPLICATIONS FOR THE INTERNAL STRUCTURE OF 67P NUCLEUS

3.1 On the organic matter in the interpretation of CONSERT and SESAME-PP results

Fig. 3 enables physical properties, such as porosity and dust content, to be related to values of ϵ' for materials including water ice and silicates as mentioned above. We have also discussed the effect on ϵ' of the presence of organic materials with respect to silicates. Because the nature of the organic materials observed in the coma or at the surface of 67P is probably different with respect to the tholins studied here, we cannot exclude that other organic materials with a different composition would act differently (see Section 2.5.1). Indeed, the solid density and the intrinsic permittivity of the organic materials have to be taken into account to interpret the values of ϵ' (Hérique et al. 2016). Further complementary measurements need to be performed with other analogues of cometary organic matter to better constrain the interpretation of the CONSERT and SESAME-PP results. Nevertheless, we can suggest that for a dust component mostly composed of organic materials, the consequence for ϵ' is that the range of porosity crossed by the ϵ' isolines presented in Fig. 3, which is valid for silicate-rich materials, would be reduced. And even with a mixture composed of organic and silicate-rich materials, the silicate-rich materials will dominate the ϵ' behaviour. That implies that the main conclusion of the interpretation of the SESAME-PP and CONSERT results, which is presented in the next section, would not be affected.

3.2 A porosity gradient in the small lobe of the nucleus

For a temperature equal to 100 K, Fig. 3 allows different values of ϵ' to be interpreted in terms of ranges of porosity, dust-mass fraction and dust-to-ice volumetric ratio. From Fig. 3, which is derived from permittivity measurements in the range of 50 MHz–2 GHz, the results obtained by CONSERT can be interpreted. Moreover, it can also be used to interpret the results obtained by SESAME-PP at lower frequencies and at temperatures below 150 K, because of the very long relaxation time of the polarization mechanisms which occur for all analogue materials at these temperatures. As mentioned in Section 2.1, during the FSS, the temperature in the interior of the small lobe of the nucleus and at the surface of Abydos site has been estimated to be less than 150 K. The initial multidimensional problem of the variation of the permittivity, as a function of the frequency, the temperature, the dust content and the porosity, can therefore be reduced to two dimensions if we assume no frequency dependence of ϵ' below 150 K and an average temperature equal to about 100 K. Thus, one can reasonably assume that the different values of the real part of permittivity reported in Kofman et al. (2015) and Lethuillier et al. (2016) are caused by a variation of the porosity of the medium and/or the composition.

The penetrator of the MUPUS package has not been able to penetrate the surface by more than 27 mm (Spohn et al. 2015), even with the maximum energy level. This behaviour would suggest the presence of a compacted material composed of ice beneath, so that one may exclude the case of a material only composed of dust and make the reasonable assumption that the dust-to-ice volumetric ratio is lower than 6 at the location of SESAME-PP measurements. The lower limit of the real part of the permittivity of the near-surface at the location of the Philae lander is equal to about 2.45 (Lethuillier et al. 2016). Fig. 3 predicts that the corresponding upper limit of the porosity of the near-surface is in the range of 18–55 per cent for a dust-to-ice volumetric ratio below 6 (i.e. a dust-mass fraction of less than 0.95). It would be equal to 58 per cent if the lower limit of the measurement performed by SESAME-PP (i.e. $\epsilon' = 2.25$) is taken into account. With the same assumption on the upper limit of the dust content, the bulk value of the real part of the permittivity of the small lobe equal to 1.27 ± 0.05 corresponds to a porosity in the range of 67–86 per cent in Fig. 3, taking into account the lower and upper limits of the measurement. Thus, from this analysis, the upper limit of the porosity of the near-surface at the location of Philae and the lower limit of the porosity of the interior of the small lobe differs, at least, by about 9 per cent.

Furthermore, the dust-to-gas mass ratio reported in Rotundi et al. (2015), i.e. equal to 4 ± 2 , may help us to better constrain the lower limit of the dust content. Indeed, this result supports the dusty nature of the nucleus. A dust-to-ice mass ratio equal to 1 seems to be a reasonable lower limit of the expected dust-to-ice mass ratio inside the nucleus. That yields a lower limit of the dust-mass fraction equal to 0.5 and a dust-to-ice volumetric ratio equal to 0.3 in

Fig. 3. In this case, the porosity deduced from the bulk value of ϵ' for the small lobe of the 67P nucleus remains in the range of 75–86 per cent. The corresponding upper limit of the porosity of the near-surface would be in the range of 32–58 per cent. These results are consistent with those obtained by Kofman et al. (2015) and Lethuillier et al. (2016). Moreover, the porosity ranges obtained by our approach and the one of Kofman et al. (2015) are consistent with the porosity ranges determined for the whole nucleus by Sierks et al. (2015, 70–80 per cent) and Pätzold et al. (2016, 70–75 per cent).

Thus, taking into account the temperatures at the surface and in the interior of the nucleus, and the possible variations of the dust content, the interpretation of the SESAME-PP and CONSERT results shows that the upper limit of the porosity of the near-surface, at Philae's location, is smaller, at least by about 9 per cent, than the porosity of the interior of the nucleus. These results suggest an increase of the porosity with the increasing depth in the small lobe of the 67P nucleus. This conclusion supports the results obtained by Ciarletti et al. (2015), who have performed electromagnetic simulations with a ray-tracing code to estimate the effect of a variation of ϵ' in the subsurface on the ability of CONSERT to receive signals during the FSS. Their results suggest an increase of the ice content or/and the porosity over a depth of the order of one hundred of metres around the location of the Philae lander. Our approach shows that an increase of the porosity with the increasing depth cannot be excluded even taking into account the variations of the composition.

Our interpretation is consistent with the conclusions presented in Lethuillier et al. (2016). The presence of an uppermost layer with different physical properties with respect to the material in depth is supported by this work. A greater porosity is highlighted for the interior of the small lobe of 67P, meaning that the near-surface may have evolved. This uppermost layer may be composed of dust and ice, probably produced by sublimation and redeposition cycles and/or sintering of ice as observed on 67P (Groussin et al. 2015) and studied with laboratory simulations (Poch et al. 2016a, and references therein). This conclusion is also supported by the low values of the material strength of the nucleus estimated by Groussin et al. (2015) which contrast with the high resistance to penetration of the hard subsurface encountered by the penetrator of the MUPUS package.

Regarding the imaginary part of the permittivity of the nucleus, from the results mentioned in Section 2.4, it would be very small, probably less than 0.01 and close to 0.001 for a porosity greater than 65 per cent at the operating frequency of CONSERT. This is consistent with the travel of the radiowaves of CONSERT through hundred of metres in the interior of the nucleus.

4 CONCLUSION

We report in this paper on a new interpretation of the values of ϵ' obtained by the SESAME-PP and the CONSERT instruments during the FSS of the *Rosetta* mission based on laboratory measurements of the permittivity of porous water ice samples and icy mixtures. SESAME-PP determined a lower limit of ϵ' , equal to 2.45 ± 0.20 , for the first metre of the near-surface of the small lobe of the 67P nucleus. The temperatures were in the range of 100–150 K at the time of the measurements at Abydos site. CONSERT determined a value of ϵ' which integrates the physical properties of the small lobe of the nucleus along the propagation path of the radiowaves at temperatures possibly near 100 K or lower. The radiowaves crossed the small lobe of the nucleus over a depth of about hundred of

metres and intersected the Maftet and Bastet regions. Morphological evidences have shown that these regions are consolidated. The physical properties of the material sounded by SESAME-PP and also MUPUS, suggesting a consolidated nature, may be extended to the Maftet and Bastet consolidated terrains intersected by the CONSERT signals. Then the real part of the permittivity in the near-surface of these terrains may also be greater than 2.

We use a semi-empirical formula taking into account the dependences of ϵ' in terms of porosity, dust content and temperature for porous and icy analogues of cometary materials to interpret the results obtained by the SESAME-PP and the CONSERT instruments. For these analogues, which consist of porous water ice samples and mixtures of water ice and JSC-1A simulant samples, a non-dispersive behaviour of ϵ' has been measured between 50 MHz and 2 GHz. Then, because of the absence of a frequency dependence and temperature dependence of ϵ' at the temperature conditions of the FFS, SESAME-PP and CONSERT results can be compared and interpreted in terms of differences in composition and/or porosity. The semi-empirical formula enables us to derive isolines of ϵ' as a function of the dust content and the porosity, at a given temperature. For a temperature below 150 K, the results suggest that, even for a very dusty material, e.g. with a dust-to-ice volumetric ratio equal to 1.9 (i.e. a dust-to-ice mass ratio equal to about 6, which is equal to the upper limit of the dust-to-gas mass ratio obtained from GIADA), the upper limit of the porosity of the near-surface of the small lobe of the nucleus 67P, at location of Philae, would be smaller at least by about 11 per cent than the porosity of the interior of the nucleus. Moreover, this difference may reach about 25 per cent if we consider the same value for the dust-to-ice volumetric ratio in the interior, even if it is very unlikely. These results indicate that the porosity increases with the increasing depth in the small lobe of the nucleus, in agreement with the results obtained from a different method of interpretation used by the SESAME-PP and CONSERT teams.

The dust component of the cometary material could be also rich in organic materials. Preliminary measurements obtained on organic materials have shown that the main conclusion would not be changed. If the dusty components of the cometary material are composed of silicate-rich materials and organic materials, then the silicate-rich materials will dominate the ϵ' behaviour. The effect of different organic materials on the permittivity has to be investigated more with complementary measurements that we expect to perform closely soon.

The presence of a hard icy layer in the near-surface of the nucleus at Philae's location, which could have been formed by successive episodes of sublimation/recondensation and/or sintering, is supported by this work. This layer contrasts with the high porosity of the material in depth in the small lobe of the nucleus inferred from CONSERT results.

ACKNOWLEDGEMENTS

Support from the Swiss National Science Foundation is acknowledged. Support from Centre National d'Étude Spatiale (CNES, France) is acknowledged for this work based on observations with CONSERT and SESAME onboard *Rosetta*. We thank Pr. Nathalie Carrasco and Pr. Cyril Szopa from LATMOS laboratory (Guyancourt/Paris, France) who provided us with the tholins samples from the PAMPRE experiment in order to perform the permittivity measurements. We acknowledge Dr Mohamed Ramy El-Maarry for the fruitful discussions about the morphology of the small lobe of 67P.

REFERENCES

- Adams R. J., Perger W. F., Rose W. I., Kostinski A., 1996, *J. Geophys. Res.*, 101, 8175
- Andersson O., 2008, *J. Phys.: Condens. Matter.*, 20, 244115
- Auger A.-T. et al., 2015, *A&A*, 583, A35
- Auster H.-U. et al., 2015, *Science*, 349, aaa5102
- Biele J. et al., 2015, *Science*, 349, aaa9816
- Bonnet J.-Y. et al., 2015, *Icarus*, 250, 53
- Brouet Y., Levasseur-Regourd A. C., Encrenaz P., Gulikis S., 2014, *Planet. Space Sci.*, 103, 143
- Brouet Y., Levasseur-Regourd A. C., Sabouroux P., Encrenaz P., Thomas N., Heggy E., Kofman W., 2015, *A&A*, 583, A39
- Brouet Y. et al., 2016, *J. Geophys. Res.*, preliminary acceptance, under review
- Calla O. P. N., Rathore I. S., 2012, *Adv. Space Res.*, 50, 1607
- Campbell M. J., Ulrichs J., 1969, *J. Geophys. Res.*, 74, 5867
- Capaccioni F. et al., 2015, *Science*, 347, aaa0628
- Carrasco N. et al., 2009, *J. Phys. Chem. A*, 113, 11195
- Ciarletti V., Levasseur-Regourd A. C., Lasue J., Statz C., Plettemeier D., Hérique A., Rogez Y., Kofman W., 2015, *A&A*, 583, A40
- Cochran A. L. et al., 2015, *Space Sci. Rev.*, 197, 9
- Coradini A. et al., 2007, *Space Sci. Rev.*, 128, 529
- Duprat J. et al., 2010, *Science*, 328, 742
- El-Maarry M. R. et al., 2015a, *Geophys. Res. Lett.*, 42, 5170
- El-Maarry M. R. et al., 2015b, *A&A*, 583, A26
- El-Maarry M. R. et al., 2016, *A&A*, in press
- Festou M. C., Keller H. U., Weaver H. A., 2004, *Comets II*. Univ. Arizona Press, Tucson, AZ
- Filacchione G. et al., 2016, *Nature*, 529, 368
- Goesmann F. et al., 2007, *Space Sci. Rev.*, 128, 257
- Goesmann F. et al., 2015, *Science*, 349, aab0689
- Gough S. R., 1972, *Can. J. Chem.*, 50, 3046
- Groussin O. et al., 2015, *A&A*, 583, A32
- Gulikis S., Allen M., von Allmen P., Beaudin G., Biver N., Bockelée-Morvan D., 2015, *Science*, 347, aaa0709
- Heggy E., Paillou P., Ruffié G., Malezieux J. M., Costard F., Grandjean G., 2001, *Icarus*, 154, 244
- Heggy E., Palmer E. M., Kofman W., Clifford S. M., Richter K., Hérique A., 2012, *Icarus*, 221, 925
- Hérique A., Rogez Y., Pasquero O. P., Zine S., Puget P., Kofman W., 2015, *Planet. Space Sci.*, 117, 475
- Hérique A. et al., 2016, *MNRAS*, in press
- Hill E., Mellin M. J., Deane B., Liu Y., Taylor L. A., 2007, *J. Geophys. Res.*, 112, 2006
- Imanaka H., Cruikshank D. P., Khare B. N., McKay C. P., 2012, *Icarus*, 218, 247
- Jost B., Pommerol A., Poch O., Gundlach B., Leboeuf M., Dadras M., Blum J., Thomas N., 2016, *Icarus*, 264, 109
- Keller H. U. et al., 2007, *Space Sci. Rev.*, 128, 433
- Klingelhofer G., Girones Lopez J., Schmanke D., Markovski C., Brückner J., d'Uston C., Economu T., Gellert R., 2015, *EGU General Assembly Conference Abstracts.*, Vienna, Austria, p. 13614
- Kofman W. et al., 1998, *Adv. Space Res.*, 21, 1589
- Kofman W. et al., 2015, *Science*, 349, aab0639
- Lethuillier A. et al., 2016, *A&A*, 591, A32
- Lide A. H., 2005, *Handbook of Chemistry and Physics*. CRC Press, Boca Raton, FL
- Mahjoub A., Carrasco N., Dahoo P.-R., Gautier T., Szopa C., Cernogora G., 2012, *Icarus*, 221, 670
- Mattei E., Lauro S. E., Vannaroni G., Cosciotti B., Bella F., Pettinelli E., 2014, *Icarus*, 229, 428
- Mätzler C., Wegmüller U., 1987, *J. Phys. D: Appl. Phys.*, 20, 1623
- Nesvorný D., Jenniskens P., Levison H. F., Bottke W. F., Vokrouhlický D., Gounelle M., 2010, *ApJ*, 713, 816
- Nicolson A. M., Ross G. F., 1970, *IEEE Trans. Instrum. Meas.*, 19, 377
- Olhoeft G. R., Strangway D. W., 1975, *Earth Planet. Sci. Lett.*, 24, 394
- Paillou P., Lunine J., Ruffié G., Encrenaz P., Wall S., Lorenz R., Janssen M., 2008, *Geophys. Res. Lett.*, 35, L18202
- Pätzold M. et al., 2007, *Space Sci. Rev.*, 128, 599
- Pätzold M. et al., 2016, *Nature*, 530, 63
- Pernot P., Carrasco N., Thissen R., Schmitz-Afonso I., 2010, *Anal. Chem.*, 82, 1371
- Pettinelli E., Vannaroni G., Cereti A., Paolucci F., Della Monica G., Storini M., Bella F., 2003, *J. Geophys. Res.*, 108, 8029
- Poch O., Pommerol A., Jost B., Carrasco N., Szopa C., Thomas N., 2016a, *Icarus*, 266, 288
- Poch O., Pommerol A., Jost B., Carrasco N., Szopa C., Thomas N., 2016b, *Icarus*, 267, 154
- Pommerol A. et al., 2015, *A&A*, 583, A25
- Quirico E. et al., 2016, *Icarus*, 272, 32
- Rotundi A. et al., 2015, *Science*, 347, aaa3905
- Sciamma-O'Brien E., Carrasco N., Szopa C., Buch A., Cernogora G., 2010, *Icarus*, 209, 704
- Sciamma-O'Brien E., Dahoo P.-R., Hadamcik E., Carrasco N., Quirico E., Szopa C., Cernogora G., 2012, *Icarus*, 218, 356
- Seidensticker K. J. et al., 2007, *Space Sci. Rev.*, 128, 301
- Sierks H. et al., 2015, *Science*, 347, aaa1044
- Sihvola A. H., 1999, *Electromagnetic Mixing Formulas and Applications*. IEE Electromagnetic Waves Series 47, London, UK
- Spohn T. et al., 2007, *Space Sci. Rev.*, 128, 339
- Spohn T. et al., 2015, *Science*, 349, aab0464
- Szopa C., Cernogora G., Boufendi L., Correia J. J., Coll P., 2006, *Planet. Space Sci.*, 54, 394
- Thomas N. et al., 2015, *Science*, 347, aaa0440
- Ulaby F. T., Long D. G., 2014, *Microwave Radar and Radiometric Remote Sensing*. Univ. Michigan Press, Ann Arbor, MI
- Yoldi Z., Pommerol A., Jost B., Poch O., Gouman J., Thomas N., 2015, *Geophys. Res. Lett.*, 42, 6205

SUPPORTING INFORMATION

Additional Supporting Information may be found in the online version of this article:

Supplementary_Materials.pdf

(<http://www.mnras.oxfordjournals.org/lookup/suppl/doi:10.1093/mnras/stw2151/-/DC1>).

Please note: Oxford University Press is not responsible for the content or functionality of any supporting materials supplied by the authors. Any queries (other than missing material) should be directed to the corresponding author for this article.

This paper has been typeset from a \LaTeX file prepared by the author.